

## 1.2 ESTIMATION OF POTENTIAL EVAPOTRANSPIRATION FROM MERGED CERES AND MODIS OBSERVATIONS

Anand K. Inamdar\* & Andrew French

USDA Arid Land Agricultural Research Center, Maricopa, Arizona

\*

### 1. INTRODUCTION

Net surface radiation is a key element of the surface energy balance with the highest degree of correlation with the evapotranspiration which is the primary process influencing the energy and water exchanges between the earth, atmosphere and biosphere (Priestley and Taylor, 1972; Monteith, 1972; Wang et al, 2007). During the last few decades several methods have been developed to estimate the net surface shortwave radiation from satellites (Tarpley, 1979; Pinker et al, 1995, Cess and Vulius, 1989; Li et al, 1993; Masuda et al, 1995 to name just a few). While empirical or statistical methods (Tarpley, 1979) are inappropriate for global implementation, the satellite-based methods (Li et al, 1995) mainly relied on broadband satellite data such as the Earth Radiation Budget Experiment (ERBE) with wide field of view sensors. The spatial resolution of ERBE (30 km at nadir) and CERES on EOS/Terra and EOS/Aqua (20 km at nadir) is too coarse for some applications such as precise management of water resources in agriculture. Unfortunately current satellite

sensors with higher spatial resolution (MODIS) have narrowband spectral channels.

In the present study, we propose to combine the advantages of well-validated CERES broadband flux algorithms for TOA (top-of-atmosphere) to surface for both shortwave (SW) and longwave (LW) with high spatial resolution MODIS data. This is a pilot study and includes many simplifications: 1) without any scene-dependent angular distribution modeling (ADM) to convert TOA radiance to flux; 2) employs limited number (only three in SW and 2 in LW) of MODIS channels and 3) includes a simplified representation of aerosol effects.

### 2. DATA SOURCES

- CERES Single Satellite Footprint (SSF) Edition 2B
- MODIS Level 1B Radiance (MOD021KM)
- MODIS Level 2 Total precipitable water (MOD05\_L2)
- MODIS Level 2 LST and Emissivity (MOD11\_L2)
- Global Aerosol Climatology Project ([gacp.giss.nasa.gov](http://gacp.giss.nasa.gov))

---

\* *Corresponding author address:* Anand K. Inamdar, ALARC, 21881 North Cardon Lane, Maricopa, AZ 85238; e-mail: [anand.inamdar@ars.usda.gov](mailto:anand.inamdar@ars.usda.gov)

The focus of our study is the semi-arid and arid regions of South West US (91 W – 126 W, 25 N – 43 N).

### 3. SHORTWAVE SCHEME

#### 3.1 MODIS Narrowband to Broadband Conversion

The CERES footprint represents the CERES Field of View (FOV), determined by its Point Source Function (PSF). PSF is a two-dimensional bell-shaped function that defines the CERES instrument response to the viewed radiation field. The SSF data provides MODIS Imager footprint radiance parameters convolved with the CERES FOV for three shortwave channels (0.644, 0.858 and 1.64  $\mu\text{m}$ ), which have been used in the narrowband-broadband TOA flux conversion.

The conversion of MODIS narrowband radiances,  $I_\lambda$ , to TOA broadband flux,  $F_{SW,TOA}$ , is accomplished using the regression relation:

$$F_{SW,TOA} = a_0 + \sum_{i=1}^3 a_i I_\lambda(i), \quad (1)$$

where the  $I_\lambda()$ 's represent MODIS radiances in the channels 0.644, 0.858 and 1.64  $\mu\text{m}$  convolved with the CERES FOV. The regression coefficients are determined using data for the month of June 2003 over the US southwest by relating MODIS narrowband radiances in the three SW channels with coincident CERES TOA flux values for discrete intervals of the solar zenith angle (10 degree increments), viewing zenith angle (10 degree increments) and relative azimuth angle (20 degree increments).

Figure 1 presents an evaluation of the regression scheme over the US southwest. The bias and root mean square errors are consistent with those reported by Loeb et al (2006).

#### 3.2 Net surface solar flux

To estimate the net solar flux, we implement the CERES SW Model A which is based on the algorithm of Li et al (1993). The net SW flux at the surface,  $\Delta F_{SW,SFC}$ , is expressed as the fraction of solar flux absorbed at the surface in terms of the TOA flux,  $F_{SW,TOA}$ , cosine of solar zenith angle ( $\mu$ ) and column precipitable water ( $w$  cm).

$$\frac{\Delta F_{SW,SFC} d^2}{E_0 \mu} = \alpha - \beta r, \quad (2)$$

where,  $r$  is the TOA albedo,  $\frac{F_{SW,TOA} d^2}{E_0 \mu}$  and the intercept ( $\alpha$ ) and slope ( $\beta$ ) are given by,

$$\alpha = 1 + a_1 \mu^{-1} + a_2 \mu^{-0.5} + [1 - \exp(-\mu)](a_3 + a_4 \sqrt{w}) \mu^{-1}$$

$$\beta = 1 + a_5 + a_6 \ln(\mu) + a_7 \sqrt{w}$$

$E_0$  is the solar constant (1365  $\text{W m}^{-2}$ ),  $d$  is the earth-sun distance in astronomical units and  $a_1, a_2, \dots, a_7$  are constants.

This has been further modified to include correction for aerosol effect (Masuda et al, 1995). The aerosol optical depth at 0.55  $\mu\text{m}$  needed to implement the the aerosol correction were obtained from the Global

Validation of the net solar flux derived from MODIS is performed (Fig. 2) by comparing with the corresponding value from CERES SW model A.

#### 4. LONGWAVE SCHEME

##### 4.1 Longwave TOA flux

There are only two imager channels available (11 and 12  $\mu\text{m}$ ) in the thermal infrared window convolved with the CERES FOV provided in the SSF data granule at present. In the absence of other non-window channels, we use column precipitable water ( $w$  cm) as an additional parameter to derive the broadband TOA LW flux. Thus if  $I_{11}$  and  $I_{12}$  represent radiances in the MODIS channels at 11 and 12  $\mu\text{m}$  respectively, then broadband TOA flux,  $F_{LW,TOA}$  can be expressed as a linear combination

$$F_{LW,TOA} = a_0 + a_1 I_{11} + a_2 I_{12} + a_3 w \quad (3)$$

The performance of the regression relation (3) using SSF parameters for June 2003 over the US southwest domain is shown in Fig. 3. We next implement a simplified form of the LW Model A (Inamdar & Ramanathan, 1997) for TOA to surface flux.

##### 4.2 Net LW Flux at Surface

The downwelling LW flux at the surface,  $F_{LW,SFC}$ , is expressed in terms of the atmospheric greenhouse effect,  $G_a$  (defined as the difference between

surface Planck blackbody emission,  $\sigma T_s^4$  and TOA LW flux, where  $\sigma$  is the Stefan-Boltzmann constant and  $T_s$  is the surface temperature) and linear and logarithmic column precipitable water amounts. The linear and logarithmic column water vapor terms account for water vapor absorption in the window (8-12  $\mu\text{m}$ ) and non-window regions of the thermal infrared spectrum (Inamdar & Ramanathan, 1997, 2004). In the formulation below, the lower case flux terms are normalized (with respect to surface blackbody emission,  $\sigma T_s^4$ ).

$$f_{lw,sfc} = a_0 + a_1 g_a + a_2 w + a_3 \ln(w) \quad (4)$$

$$g_a = \frac{\sigma T_s^4 - F_{LW,TOA}}{\sigma T_s^4} \quad \&$$

$$F_{LW,SFC} = f_{lw,sfc} (\sigma T_s^4)$$

Fig. 4 presents scatter plot of downwelling LW flux from CERES and that predicted by regression relation (4).

#### 5. CONCLUSIONS

Techniques have been developed for estimation of net surface radiation, the key input in the derivation of evapotranspiration and land surface - atmosphere energy exchange, from MODIS narrowband radiances employing CERES broadband data as a calibration source. The present study is preliminary with the number of MODIS channels limited to those convolved with the CERES FOV in SSF data. Results show potential for accurate satellite-based determination of land surface energy exchange components at high spatial resolution on a global scale.

Future enhancements will include 1) convolution of additional MODIS channels with CERES FOV; 2) implementation of scene-dependent Angular Distribution Models for radiance to flux conversion; 3) better representation of aerosols and 4) use of GOES Imager visible channel to perform temporal interpolation.

**Acknowledgements:** This research was supported by NASA Grant EOS/03-0057-0459.

## References

Cess, R.D., and I.L. Vulijs, 1989: Inferring surface solar absorption from broadband satellite measurements. *Journal of Climate*, 2, 974-985.

Li, Z., H.G. Leighton, and R.D. Cess, 1993: Surface net solar radiation estimated from satellite measurements: Comparisons with tower observations. *Journal of Climate*, 6, 1764-1772.

Masuda, K., H.G. Leighton, and Z. Li, 1995: A new parameterization for the determination of solar flux absorbed at the surface from satellite measurements. *Journal of Climate*, 8, 1615-1629.

Monteith, J.L., 1972: *Principles of Environmental Physics*. 241 pp., Edward Arnold, London.

Pinker, R.T., R. Frouin, and Z. Li, 1995: A review of satellite methods to derive surface shortwave albedo. *Remote Sens. Environ.*, 51, 105-124.

Priestley, C.H.B., and R.J. Taylor, 1972: On the assessment of surface heat flux and evaporation using large-scale parameters. *Mon. Wea. Rev.*, 100, 81-92.

Tang, B., Z. Li, and R. Zhang, 2006: A direct method for estimating net surface shortwave radiation from MODIS data. *Remote Sens. Environment*, 103, 115-126.

Tarpley, J.D., 1979: Estimating incident solar radiation at the surface from geostationary satellite data. *J. Appl. Meteor.*, 18, 1172-1181.

Wang, K., P. Wang, Z. Li, M. Cribb, and M. Sparrow, 2007: A simple method to estimate actual evapotranspiration from a combination of net radiation, vegetation index, and temperature. *J. Geophys. Res.*, 112, doi:10.1029/2006JD008351.

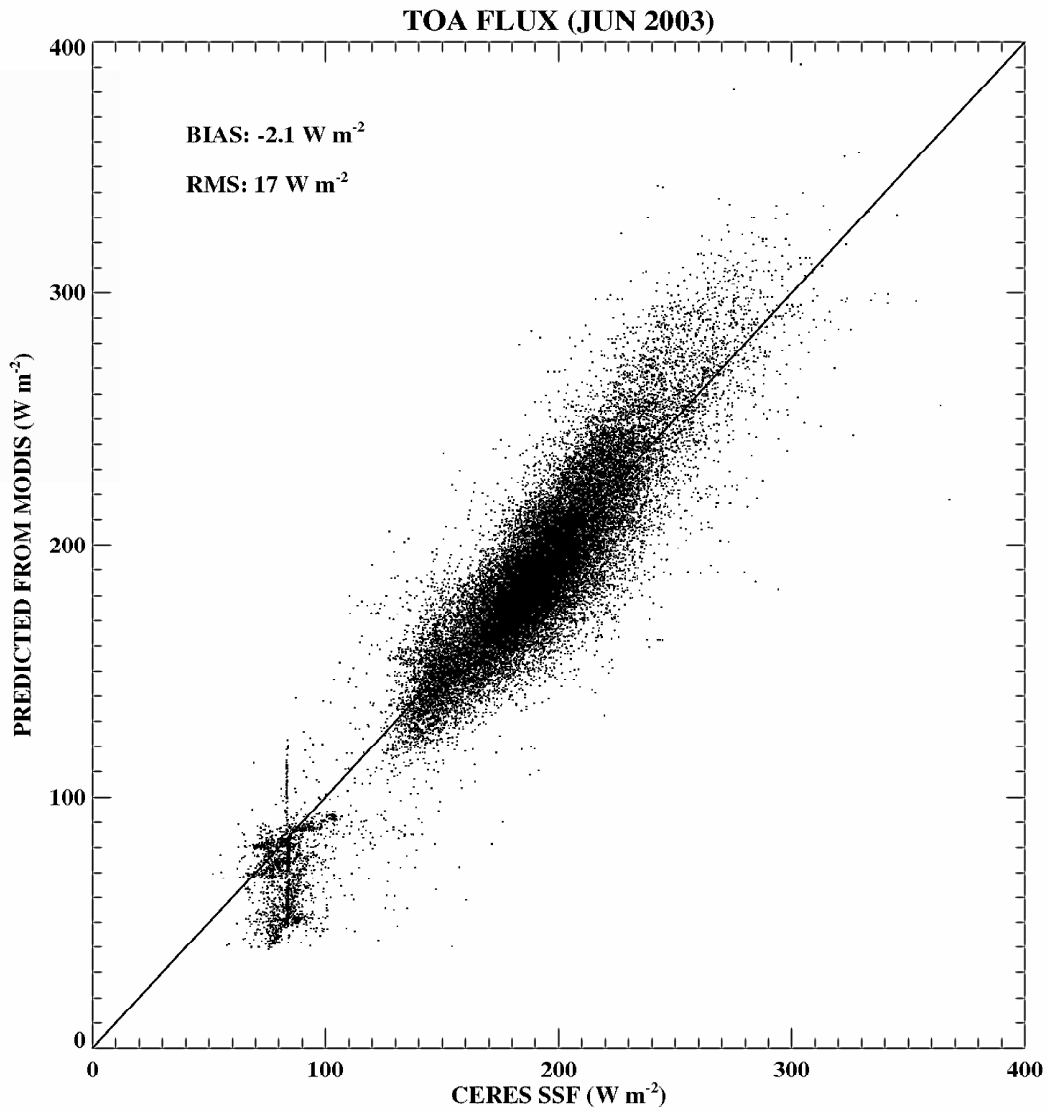


Fig. 1. Comparison of TOA SW flux from MODIS narrowband radiances with coincident value obtained from CERES SSF data (Eq. 1)

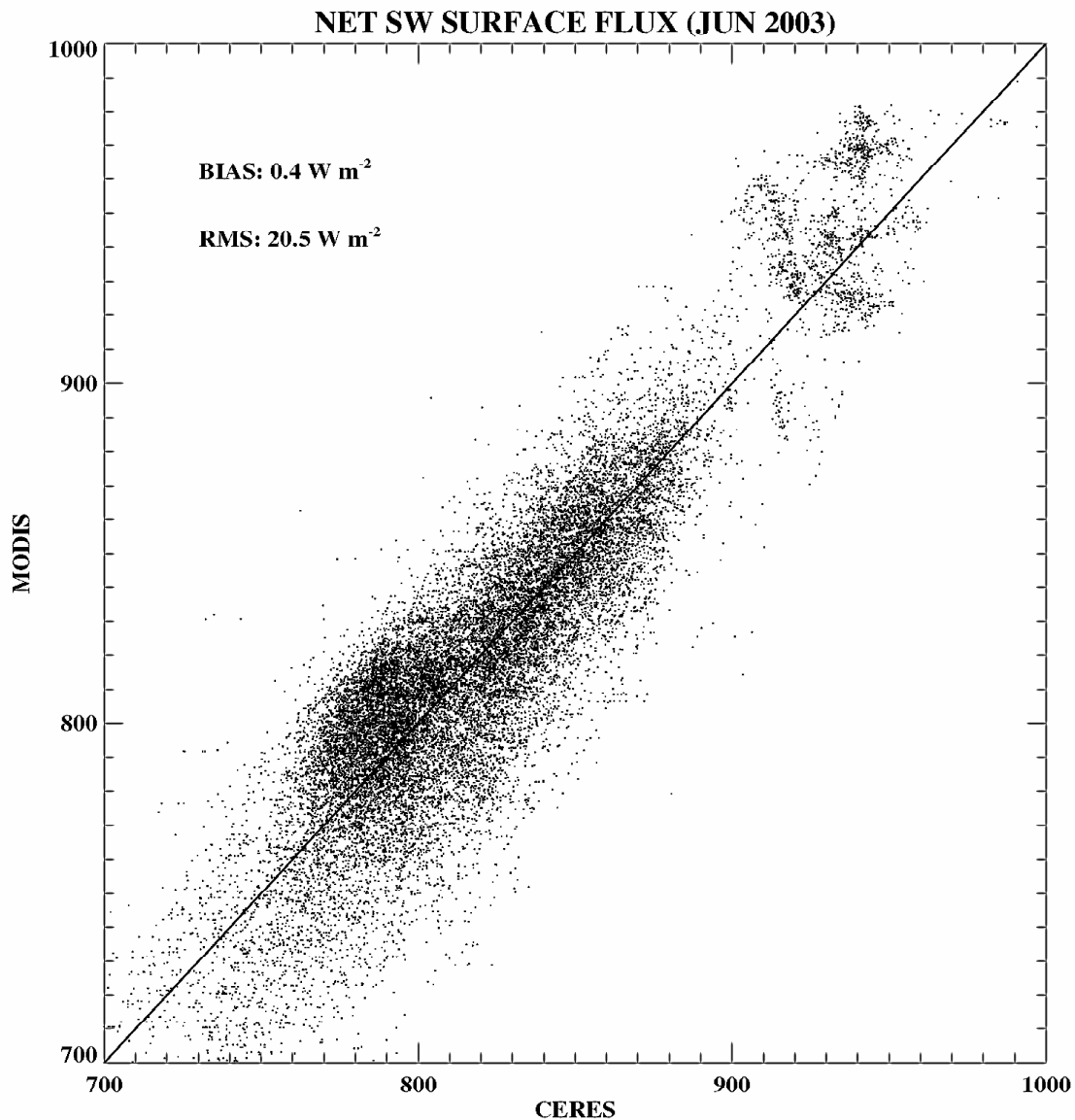


Fig. 2. Net SW surface flux obtained by applying Eq. (2) to MODIS-derived TOA SW flux. The total column precipitable water for each 1 km MODIS pixel has been derived from disaggregated MOD05 IR water vapor product. To facilitate comparison with CERES, MODIS-derived net surface flux has been binned into 0.1 degree lat-lon bins.

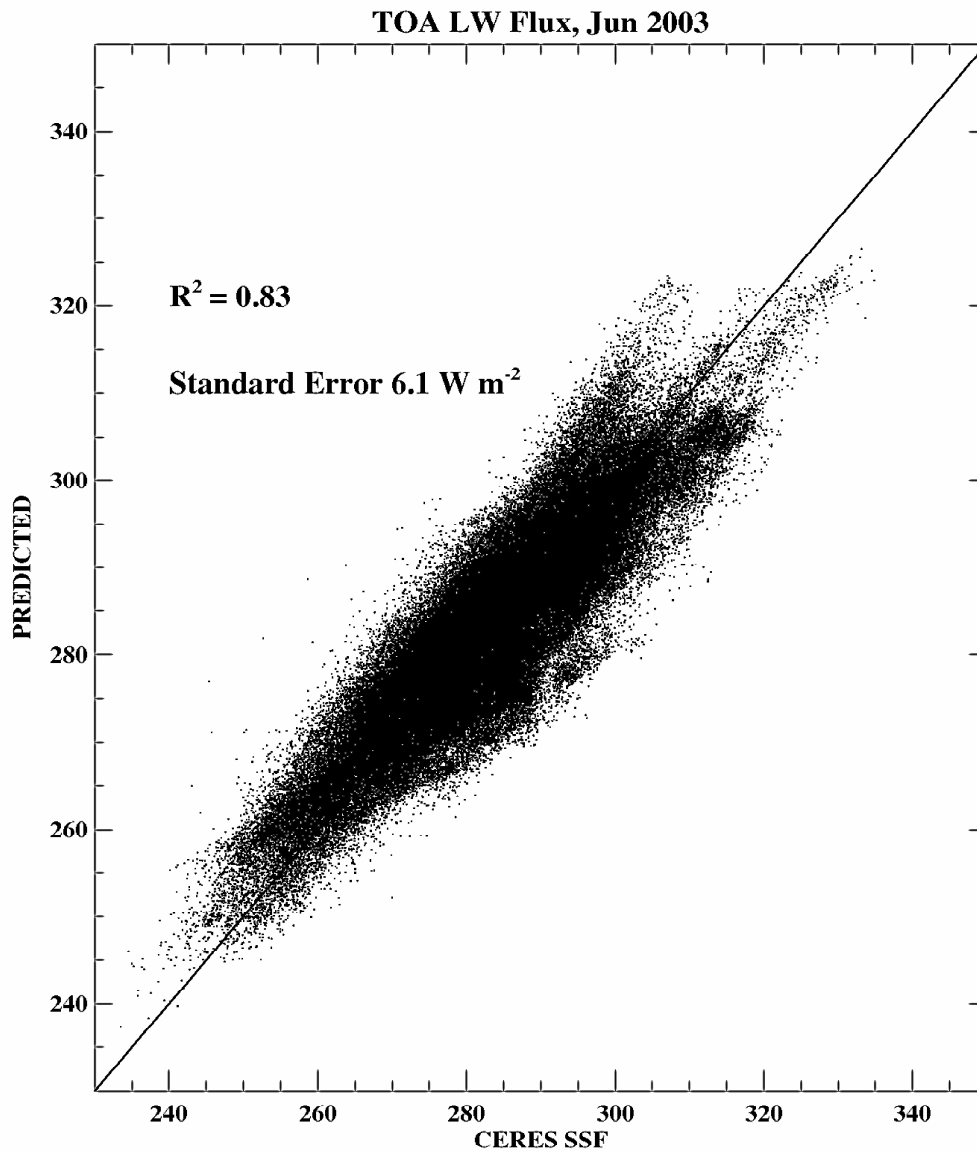


Fig. 3. Performance of the regression relation (3) for broadband LW TOA flux in terms of convolved imager radiances in the thermal infrared bands and column precipitable water.

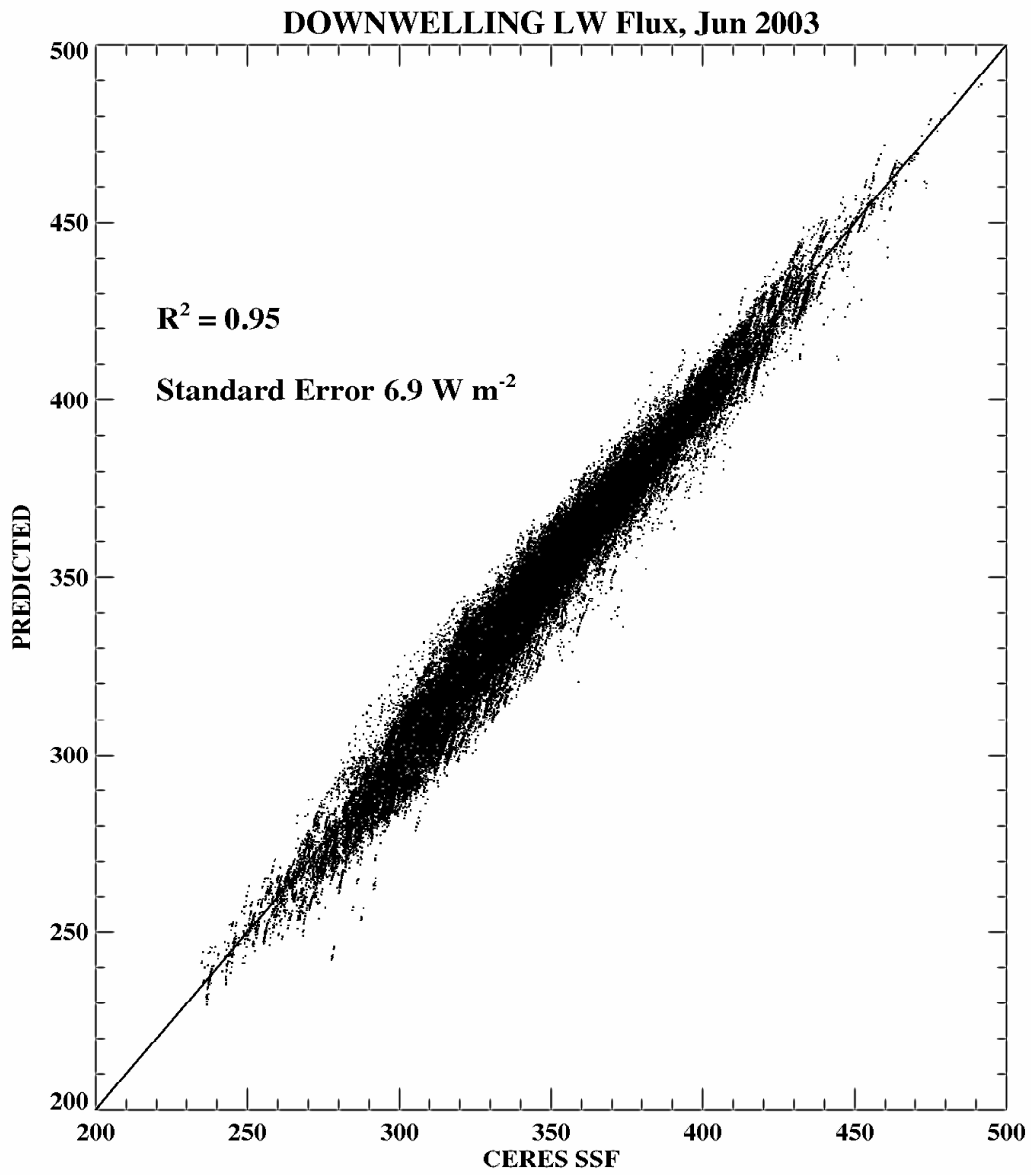


Fig. 4. Scatter plot of downwelling LW flux from CERES SSF (Model A) and that predicted from the simplified regression scheme (Eq. 4).